

MEMBERSHIP PRIVACY RISKS OF SHARPNESS AWARE MINIMIZATION

Young In Kim

Department of Computer Science
 Purdue University
 West Lafayette, IN 47906, USA
 kim3531@purdue.edu

Pratiksha Agrawal

Department of Computer Science
 Purdue University
 West Lafayette, IN 47906, USA
 agraw180@purdue.edu

Rajiv Khanna

Department of Computer Science
 Purdue University
 West Lafayette, IN 47906, USA
 rajivak@purdue.edu

Andrea Agiollo

Department of Computer Science
 Delft University of Technology
 Delft, Netherlands
 A.Agiollo-1@tudelft.nl

Johannes O. Royset

Department of Industrial and
 Systems Engineering
 University of Southern California
 Los Angeles, CA 90015, USA
 royset@usc.edu

ABSTRACT

Optimization algorithms that seek flatter minima such as Sharpness-Aware Minimization (SAM) are widely credited with improved generalization. We ask whether such gains impact membership privacy. Surprisingly, we find that SAM is more prone to membership inference attacks than classical SGD across multiple datasets and attack methods, despite achieving lower test error. This is an intriguing phenomenon as conventional belief posits that higher membership privacy risk is associated with poor generalization. We conjecture that SAM is capable of memorizing atypical subpatterns more, leading to better generalization but higher privacy risk. We empirically validate our hypothesis by running extensive analysis on memorization and influence scores. Finally, we theoretically show how a model that captures minority subclass features more can effectively generalize better *and* have higher membership privacy risk.

1 INTRODUCTION

Sharpness-Aware Minimization (SAM) has emerged as a prominent optimization technique for improving generalization in deep learning by encouraging flatter minima – i.e., similar loss values for weight perturbations of certain degree around the optima – in the loss landscape (Norton & Royset, 2021; Foret et al., 2020; Wu et al., 2020; Kim et al., 2022; Du et al., 2022; Kwon et al., 2021). Flatter optima are associated with robustness to weight perturbations and have been linked to reduced overfitting and improved test performance (Chen et al., 2023; Foret et al., 2020; Baek et al., 2024).

Models that generalize well are thought to rely less on memorizing specific training examples, which should also improve privacy. Consider membership inference attacks (MIAs) in which an attacker exploits the model confidence gap between training and unseen data to infer if a data point was part of the training data or not (Shokri et al., 2017). Intuitively, when a model strongly overfits (training error \ll test error), MIA would become easier. Yeom et al. (2018) formally showed that, under certain assumptions, the advantage of a threshold-based MIA is upper bounded by the model’s generalization error. In light of this conventional wisdom, one would naturally expect that a technique like SAM – which demonstrably improves generalization – should also decrease a model’s susceptibility to MIAs.

Table 1: Attack accuracy of different types of MIA on SGD, SAM and Sharp showing tradeoffs in test accuracy and MIA attacks. SAM is more prone to MIA attack. In **blue** we highlight the best performing model on the test set and in **red** the model against which MIA is more successful.

Dataset	Algo	NN	Confidence	Entropy	M-entropy	Test Acc
CIFAR-100	SGD	76.62%	77.19%	76.61%	77.30%	80.30%
	SAM	77.99%	79.10%	78.66%	79.25%	81.60%
	Sharp	57.62%	59.69%	57.88%	59.69%	76.14%
CIFAR-10	SGD	50%	59.37%	59.09%	59.51%	96.00%
	SAM	50.08%	61.64%	61.64%	61.70%	96.72%
	Sharp	50.22%	52.86%	52.47%	52.78%	92.86%
Purchase-100	SGD	66.00%	66.76%	64.78%	67.13%	85.50%
	SAM	66.62%	67.30%	65.35%	67.54%	85.54%
	Sharp	59.58%	60.96%	58.04%	61.16%	84.31%
Texas-100	SGD	59.81%	65.20%	55.74%	65.13%	50.83%
	SAM	59.56%	66.59%	57.14%	65.42%	51.34%
	Sharp	51.11%	59.89%	53.46%	59.36%	49.97%
EyePacs	SGD	73.62%	73.40%	68.50%	73.40%	73.67%
	SAM	77.73%	77.07%	73.37%	77.36%	75.41%
	Sharp	67.29%	66.67%	58.84%	66.75%	69.8%

Our work uncovers a striking contradiction to this expectation: we find that models trained with SAM are actually *more* vulnerable to MIAs than SGD consistently across diverse datasets and attack methods, even as they achieve better generalization (see Table 1 and Section 3). This result prompts a deeper investigation into the relationship between generalization, memorization, and privacy to unearth this phenomenon both empirically and theoretically.

MIA fundamentally relies on the idea that models behave differently on data points that were part of the training set versus those that were not. This gap is often attributed to overfitting, but it can be more precisely quantified using *memorization scores* (Feldman, 2020; Feldman & Zhang, 2020), defined via Leave-One-Out (LOO) error. Memorization scores measure the change in model performance when a specific training sample is removed, and thus serve as a proxy for how much the model has memorized that sample. Motivated by this connection, we analyze the memorization scores of SAM-trained models and find that *SAM exhibits higher memorization scores than SGD*, indicating stronger reliance on individual training samples. While this increased memorization provides a plausible explanation for SAM’s heightened vulnerability to MIA, it raises a key question: “How can a model that memorizes more generalize better?”

We hypothesize that the answer lies in *what* is being memorized. Under overparameterization (Allen-Zhu et al., 2019), models can memorize not only noise in the data, but also atypical patterns in under-represented subpopulations—i.e., few white tiger images with numerous yellow tiger images. This distinction is important as real world datasets are known to have a long tail of such rare subclasses (Feldman, 2020). We conjecture that SAM is capable of doing more structured memorization, selectively focusing on atypical subclass patterns, which contributes positively to generalization. Corroborating this hypothesis, we observe that SAM’s memorization score distribution is concentrated in the mid range, rather than the high end—which is typically associated with noise memorization (refer to Section 4.1). This suggests that SAM emphasizes samples that are neither trivially learned nor purely noisy, but instead represent rare, but generalizable sub-patterns.

To further validate this finding, we analyze influence scores—which measure the impact of individual training samples on test predictions (see Section 4.2). Our results show that, for SAM, samples corresponding to moderate memorization exert higher influence on test predictions compared to SGD, confirming that SAM’s generalization gains derive from its ability to better memorize rare sub-patterns rather than noise. This property benefits generalization, but comes at the cost of increased membership privacy risk due to the increased retention of information an attacker can exploit.

We support our intuition further by introducing a novel metric that quantifies the degree of memorization involved in predicting a test sample in Section 4.3. Using this metric, we dissect SAM’s performance gains and identify that SAM’s improvements mostly stem from its performance on atypical test samples that depend heavily on a handful of memorized training points. Meanwhile, SGD performs better on typical samples that rely more on broadly learned features, once again confirming the increased MIA risks associated with SAM.

Finally, we complement our empirical findings with a theoretical analysis (Section 5) that formalizes the relationship between generalization and MIA risk. We consider a data setup comprising (i) majority subclass, (ii) minority subclass, and (iii) pure noise samples, and show that even a linear classifier model that better captures minority subclass features can achieve higher generalization and higher vulnerability to MIA. This theoretical framework provides insight into when and why the conventional belief that better generalization implies lower privacy risk can break down.

Contributions In summary, our contributions are the following: (i) we are the first to empirically demonstrate that SAM-trained models exhibit higher membership privacy risk than SGD-trained models, challenging the conventional assumption that improved generalization implies stronger privacy; (ii) we compute and release memorization and influence scores for SAM-trained models; (iii) we offer a detailed and conceptually grounded analysis of the root causes of SAM’s generalization-memorization relationship; (iv) we introduce a novel methodology to dissect generalization gains, proving that SAM’s generalization gains stem from its performance on unseen atypical samples; and (v) we present a theoretical formulation showing that, under a mixture data distribution, a model can simultaneously achieve high generalization and high MIA.

2 BACKGROUND & PRELIMINARIES

Memorization & Influence scores For a training algorithm \mathcal{A} that is used to train the model $f(\cdot)$ using dataset $\mathcal{D} = ((\mathbf{x}_1, y_1), \dots, (\mathbf{x}_n, y_n))$, the amount of label memorization by \mathcal{A} on a sample $(\mathbf{x}_i, y_i) \in \mathcal{D}$ is defined by Equation (1). The probability is taken over randomness of the algorithm such as weight initialization.

$$mem(\mathcal{A}, \mathcal{D}, i) := \Pr_{f \leftarrow \mathcal{A}(\mathcal{D})} [f(\mathbf{x}_i) = y_i] - \Pr_{f \leftarrow \mathcal{A}(\mathcal{D} \setminus (\mathbf{x}_i, y_i))} [f(\mathbf{x}_i) = y_i] \quad (1)$$

Influence score of a training example (\mathbf{x}_i, y_i) on test example (\mathbf{x}'_j, y'_j) is defined by:

$$infl(\mathcal{A}, \mathcal{D}, i, j) = \Pr_{f \leftarrow \mathcal{A}(\mathcal{D})} [f(\mathbf{x}'_j) = y'_j] - \Pr_{f \leftarrow \mathcal{A}(\mathcal{D} \setminus (\mathbf{x}_i, y_i))} [f(\mathbf{x}'_j) = y'_j] \quad (2)$$

Sharpness Aware Minimization (SAM) Consider a model $f : X \rightarrow Y$ parameterized by a weight vector \mathbf{w} and a per-sample loss function $l : W \times X \times Y \rightarrow \mathbb{R}_+$. Given a dataset $S = \{(\mathbf{x}_1, y_1), \dots, (\mathbf{x}_n, y_n)\}$ sampled i.i.d. from a data distribution, the training loss is defined as $L_S(\mathbf{w}) = \sum_{i=1}^n l(y_i, f(\mathbf{x}_i, \mathbf{w}))/n$. Sharpness Aware Minimization combines traditional loss with sharpness term to minimize the difference between maximum loss in the vicinity (a Ball of radius ρ : $B(\rho)$) of the current minima. Formally, it is defined as the following:

$$L_{SAM}(\mathbf{w}) = \min_{\mathbf{w}} L_S(\mathbf{w}) + [\max_{\epsilon \in B(\rho)} L_S(\mathbf{w} + \epsilon) - L_S(\mathbf{w})] = \min_{\mathbf{w}} \max_{\epsilon \in B(\rho)} L_S(\mathbf{w} + \epsilon) \quad (3)$$

2.1 MEMBERSHIP INFERENCE ATTACKS

Let’s say that a classifier $f_v(\mathbf{x}; \theta)$ was trained using dataset $D \sim \mathcal{D}$. We call this learnt model as the victim model. There is an attacker who is given a sample data point (\mathbf{x}, y) and infers whether $(\mathbf{x}, y) \in D$ (member) or $(\mathbf{x}, y) \notin D$ (non-member). The attacker trains a model $f_a(\mathbf{x}, y) \in \{0, 1\}$ that outputs 1 for member and 0 for non-member. Based on the attacker’s knowledge about the victim model, there are many variations of the attack (Hu et al., 2022). In this paper, we consider a black-box attack scenario assuming the attacker only has access to the output probabilities of the victim model.

The most commonly used MIA is directly querying the target sample and using the statistics returned by the model to predict members and non-members of the training data with reasonable accuracy (Shokri et al., 2021; Murakonda & Shokri, 2020; Nasr et al., 2019; Zhang et al., 2021; Long et al., 2017; Sablayrolles et al., 2019; Yeom et al., 2020). Further details are provided in Section D.2.

Given n_m member data points and n_{nm} non-member data points, the empirical accuracy of a MIA is defined as the average of (i) the fraction of member samples correctly predicted as members, and (ii) the fraction of non-member samples correctly predicted as non-members. Formally:

$$\text{Acc}_{\text{MIA}} = \frac{1}{2n_m} \sum_{i=1}^{n_m} [f_a(\mathbf{x}_i, y_i) = 1 \mid (\mathbf{x}_i, y_i) \in D] + \frac{1}{2n_{nm}} \sum_{j=1}^{n_{nm}} [f_a(\mathbf{x}_j, y_j) = 0 \mid (\mathbf{x}_j, y_j) \notin D]. \quad (4)$$

3 PRIVACY RISKS OF SAM

Inspired by the link between SAM and generalization and how MIAs should exploit poor generalization, we here scrutinize the membership privacy risk of SAM by comparing the membership attack accuracy (see Equation (4)) of different MIAs against SAM- and SGD-trained models across five different benchmark datasets. Moreover, to further investigate the connection between flatness of minima and membership privacy, we also design a novel optimizer, namely *Sharp*, that explicitly aims to find sharper minima. The objective function of Sharp is,

$$\mathcal{L}_{\text{Sharp}}(\mathbf{w}) = L(\mathbf{w}) - \beta \max_{\epsilon \in B(\rho)} L(\mathbf{w} + \epsilon). \quad (5)$$

This objective can be seen as minimizing the loss at current w while maximizing the loss in the vicinity. We empirically verify that this objective does lead to a sharper minima measuring its hessian trace. Results and discussion about Sharp are available in Section F.4.

We utilize datasets and target models that are widely employed in studies on MIAs and defenses (Yeom et al., 2018; Fang & Kim, 2024; Chen et al., 2022; Jia et al., 2019). Furthermore, we assume that the attacker has access to some portion of the training data and non-training data that it uses to train the attack models—a common assumption in the MIA literature.

Datasets We use CIFAR-10, CIFAR-100 and Purchase-100 along with two medical datasets Texas-100 and EyePacs. We follow Tang et al. (2022) to determine the partition between training and test data and to determine the subset that constitutes the attacker’s prior knowledge¹. More details about the datasets and the experimental setup can be found in Section E.

Methods For each setting, we train a set of models and choose the one achieving highest validation accuracy. We then employ different MIA methods – namely NN-based, confidence-based, entropy-based and modified entropy-based attacks (see Section D.2 for a detailed formulation of each MIA) – to evaluate the attack accuracy on the target model. All details about the experimental settings can be found in Section F.

Results We report the attack accuracy and test accuracy for each model in Table 1. We report the mean accuracy over 5 randomized runs with different attack data splits. We observe that while SAM achieves the highest generalization performance, it also incurs in the highest attack accuracy for most datasets and attack methods. Moreover, the MIA gap is more pronounced for image datasets like CIFAR-10, CIFAR-100, and EyePacs than for tabular datasets. This finding is consistent with Feldman & Zhang (2020), since image datasets tend to be characterized by more long-tailed distributions composed of multiple atypical subclasses (see Section 4.3). The results also show that membership inference attack accuracy decreases for models trained with Sharp (Equation (5)) w.r.t. both SAM and SGD. On the other hand, the test accuracy for Sharp is also lower. This result suggests a strong connection between membership privacy and flatter minima in general.

Finally, to confirm that these results are not model-dependent, we report an ablation study in Section G and verify that similar findings can be observed for different model architectures over the same datasets.

¹We adopt and extend the code in <https://github.com/inspire-group/MIAfenseSELENA>

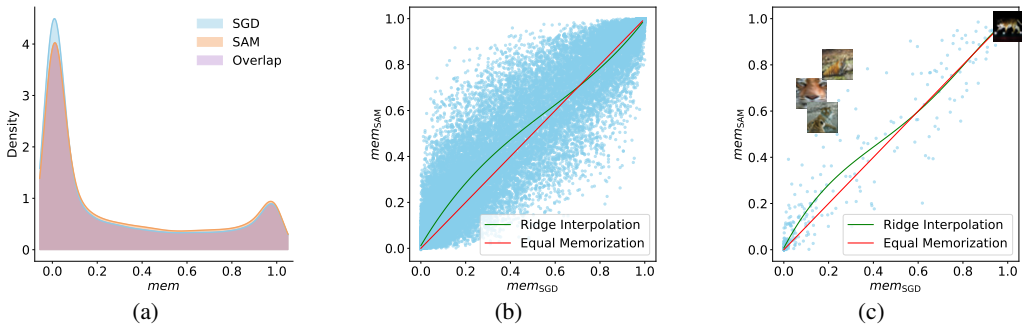


Figure 1: (a): Memorization score density plot for SAM vs SGD. SAM has less density in the lowest range, but more density spread evenly across the remaining range. (b): Memorization scores of CIFAR-100 training samples under SAM and SGD. The regression curve (in green) shows a consistent deviation from the identity line (in red), indicating that SAM memorizes a larger subset of samples in the lower score range which are likely to be atypical subclass samples. (c): Visualization of samples more memorized by SAM for the tiger class following the same setting of (b).

4 SAM LEARNS ATYPICAL SUBCLASS FEATURES MORE

To investigate the source of SAM’s increased membership privacy risk, we analyze its optimization behavior through the lens of memorization and sample influence. We follow the procedure of Feldman & Zhang (2020) to compute the memorization and influence scores for SAM-trained models on CIFAR-100. We then compare these scores against the publicly available scores for SGD-trained models on the same dataset², enabling a direct comparison of sample-level behavior between the two optimizers.

4.1 SAM MEMORIZES ATYPICAL SUB-PATTERNS MORE

We first focus on comparing the memorization behavior of SAM and SGD. Figure 1(a) shows kernel density estimates of memorization scores for both models. Although the overall shapes of the distributions are similar – reflecting the long-tailed nature of the dataset –, SAM exhibits a lower density at the lowest end of the spectrum, with the mass redistributed more evenly across the rest of the range. This indicates that SAM assigns higher memorization scores more broadly, suggesting a structured memorization of more diverse patterns compared to SGD.

To further investigate this behavior, we plot the memorization scores of individual CIFAR-100 samples under both SAM and SGD in Figure 1(b). Each sample is represented as a blue dot, with its x- and y-coordinates corresponding to its memorization score under SGD and SAM, respectively. The red diagonal line denotes equal memorization across both optimizers. Samples above this line and to the left (top-left quadrant) are more memorized by SAM, while those below and to the right (bottom-right quadrant) are more memorized by SGD.

A regression analysis over all samples – shown via the green curve – reveals a consistent deviation from the identity – red – line, skewed towards the top-left quadrant. This indicates a systematic increase in memorization for a large subset of samples under SAM. Crucially, this deviation is not concentrated at the high end of the memorization spectrum. This finding – together with the kernel density plot – supports our hypothesis that SAM does not simply memorize noise, but rather focuses on non-dominant, atypical subclass patterns that are underrepresented in the training distribution. Indeed, if SAM were memorizing sample-specific noise, we would expect a sharp concentration of kernel density at the highest end of the spectrum and a deviation of the regression curve in the top-right quadrant.

Figure 1(c) illustrates this phenomenon within the *tiger* class. Samples with higher SAM memorization relative to SGD (top-left region) tend to depict clean samples containing atypical sub-patterns—e.g., close-ups of tiger heads, tigers in water, or multiple tigers in a single image. These are visually

²<https://pluskid.github.io/influence-memorization/>

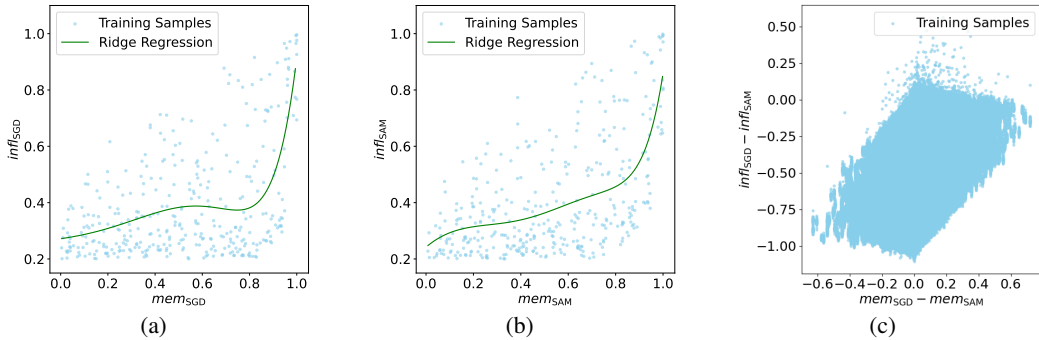


Figure 2: (a) and (b): Distribution of the influence scores of the 20 training samples achieving the highest influence score over each memorization interval over their memorization scores for SGD (a) and SAM (b). The regression analysis (green lines) shows that SAM maintains a smoother influence distribution, amplifying mid-to-high memorization samples (subclass features), while SGD relies more heavily on a narrow set of highly memorized points (noise). (c) Difference in influence scores between SAM and SGD as a function of memorization score differences. SAM downweights low-memorized samples and selectively amplifies the influence of mid-to-high memorization samples.

distinct yet semantically consistent with the class label. In contrast, samples with high memorization under both SAM and SGD (top-right region) often contain sample-specific noise, – e.g., a tiger with shiny paws on a pitch-black background –, which are less likely to generalize.

4.2 SAM INCREASES INFLUENCE OF HIGH MEMORIZATION SAMPLES

We here analyze how memorization affects the influence of training samples on test predictions, using the influence metric defined in Equation (2) for both SGD and SAM. Following the setup of Feldman & Zhang (2020), we first filter training–test sample pairs with influence scores above 0.2 to exclude non-influential cases. We then group training samples by memorization intervals – defined as $l < \text{mem}(\mathcal{A}, \mathcal{D}, i) < u$, with l and u ranging from 0 to 1 in steps of 0.05 — and, for each interval, we select the 20 training samples achieving the highest influence score on test data. This yields a distribution of influence scores of the most influential training samples conditioned on their memorization levels.

Figures 2(a) and 2(b) show the resulting distributions for SGD and SAM, respectively. As in Figure 1(b), we fit a regression curve (green line) to highlight the trends. For SGD, influence scores incur in a steep transition from lowly influent samples to highly influent points at the upper end of the memorization spectrum. This indicates SGD’s reliance on a very narrow set of highly memorized samples. In contrast, SAM exhibits a smoother transition curve, with a larger set of high (and mid-to-high) memorization samples contributing more consistently to test predictions. This supports our earlier finding that SAM emphasizes a set of atypical, non-dominant subclass patterns rather than focusing on sample-specific noise.

To further validate this, we examine the difference in influence scores between SAM and SGD as a function of their memorization score differences (Figure 2(c)). Training samples which are more memorized by SGD tend to have lower influence under SAM, suggesting that SAM down-weights the influence of its low-memorized samples. Conversely, samples with similar memorization under both optimizers but higher influence under SAM tend to lie in the mid-to-high memorization range. These are precisely the samples containing atypical subpatterns that SAM selectively amplifies, confirming our intuitions.

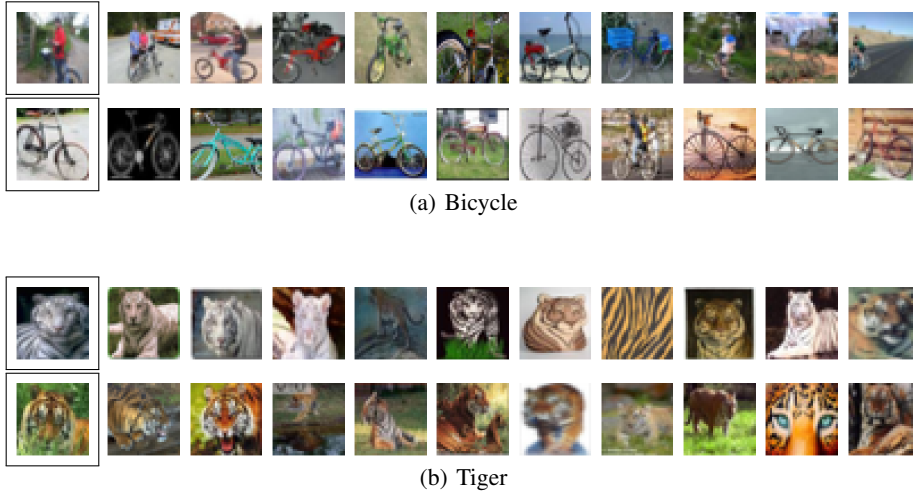


Figure 3: Test images (boxed) from buckets 1 and 5 and their respective top-10 influential training images. For each object the top row is an image from bucket 1 and the bottom row is an image from bucket 5. For bucket 1 images (higher memorization, top row), notice that the images are atypical for their classes, and there is a near duplicate in the training data that was important for generalizing on this test image. For bucket 5 images, on the other hand, the top influential images are reminiscent of the test image at a conceptual level.

4.3 SAM’S GENERALIZATION GAIN COMES FROM HIGHER MEMORIZATION OF SUB-PATTERNS

In this section, we dissect the generalization gains of SAM at a finer granularity by constructing a metric that divides the test data points into groups based on the amount of memorization used for predicting them. We then compare the performance on each group between SGD and SAM.

We measure the typicality of a test data point as the entropy of its corresponding training samples’ influence scores. We rely on this measure since, in practice, the prediction of a typical unseen sample would be evenly influenced by numerous training data points within the same class (for both SGD and SAM), while atypical counterparts would be heavily influenced by a handful of training samples that are themselves also atypical (for SGD) or by a larger set of training samples containing atypical sub-patterns (for SAM). To measure the even spread, we normalize the influence scores and leverage entropy. Even influence spread would follow a more uniform distribution resulting in high entropy, while uneven spread incurs low entropy. Formally, for each test data point i , let \mathcal{S}_i be the set of influence scores of all the training points in the same class. Let $S_{i,j}$ be the influence score of j th training point and m be the number of training points in the same class. Then, our entropy metric \mathcal{I}_{ent} is defined as:

$$\mathcal{I}_{ent}[i] = \sum_{j=1}^m -p_{i,j} * \log p_{i,j}, \text{ where, } p_{i,j} = \frac{S_{i,j}}{\sum_j S_{i,j}} \quad (6)$$

We group test data points into 5 buckets in the order of lowest \mathcal{I}_{ent} to highest \mathcal{I}_{ent} . We present some test images and their top-10 influential training images in Figure 3 from bucket 1 and bucket 5. The figure illustrates that images from bucket 1 tend to be atypical images – e.g., bicycle alongside people, white tiger, etc., – for their respective labels while images from bucket 5 tend to be more typical images—e.g., typical bicycle and yellow tiger. For quantitative verification, we plot the distribution of memorization scores of the highest influencing training points from each bucket. We observe that lower (higher) numbered buckets are influenced by training points with higher (lower) memorization scores (see Figures 4(b) and 4(c)). The results for other buckets interpolate between those of bucket 1 and 5, and are skipped for brevity.

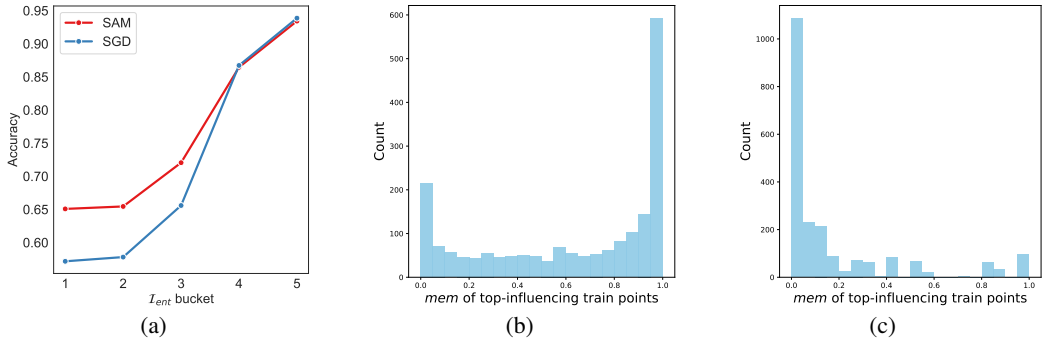


Figure 4: (a): Test accuracy on \mathcal{I}_{ent} groups as evaluated by equation 6. SAM’s performance gains comes from it correctly predicting more atypical data points that need memorization of atypical sub-patterns to be classified correctly. (b) and (c): Distribution of top-1 most influential training point’s memorization scores for \mathcal{I}_{ent} buckets 1 and 5. Testing samples falling in the lower (higher) numbered buckets are influenced by training points with higher (lower) memorization.

We compare the generalization gains of SAM against SGD on each of these buckets and show the results in Figure 4(a)³. For test data points in bucket 5, SGD achieves a negligible performance gain, while for bucket 1 SAM achieves a significant gain w.r.t. SGD. Thus, the performance gains of SAM can be attributed to it correctly predicting more atypical data points which need more memorization of atypical sub-patterns to be classified correctly. For further validation, we generate a synthetic dataset and illustrate SAM’s capability of learning atypical subclasses better than SGD in Section B.

Summary of experimental findings These results – together with the ones obtained in Sections 4.1 and 4.2 – provide strong empirical evidence that *SAM’s increased performance derives from an increased targeted memorization which focuses on atypical but informative subclass patterns that enhance generalization over atypical test data*. This explains both SAM’s improved test performance and its increased vulnerability to membership inference attacks, as these memorized patterns make training samples more distinguishable from unseen data.

5 THEORETICAL ANALYSIS

In this section, we theoretically analyze a setting involving majority subclass samples, minority subclass samples, and pure noise samples to illustrate how an overfitting model that generalizes better can also carry higher membership privacy risk. Driven by the motivations in the previous sections, we discern a model by the amount of minority subclass feature it captures. Theorem 1 shows that this property leads to higher generalization. Moreover, Theorem 2 shows that this property can also lead to higher membership privacy risk, completing our analysis. We consider perfectly interpolating linear predictors for a binary classification task. The full proofs are deferred to Section C.

Definition 1 (Data Model). *Training dataset $D = \{(\mathbf{x}_i, y_i)\}_{i=1}^n$ is sampled i.i.d. from the data distribution \mathcal{D} . We define $\mathbf{x} = [\mathbf{x}_1, \mathbf{x}_2, \mathbf{x}_3]$, $y \in \{\pm 1\}$, $\mathbf{x}_1 \in \mathbb{R}^{d_1}$, $\mathbf{x}_2 \in \mathbb{R}^{d_2}$, $\mathbf{x}_3 \in \mathbb{R}^{d_3}$. We consider a overparameterized regime where $d_1, d_2, d_3 \gg n$. We consider a linear predictor for classification, $f_{\mathbf{w}}(\mathbf{x}) = \text{sign}\{\langle \mathbf{w}, \mathbf{x} \rangle\}$ with $\mathbf{w} = [\mathbf{w}_1, \mathbf{w}_2, \mathbf{w}_3]$. We assume perfect interpolation satisfying finite margin $\forall i \ 0 \leq m_0 \leq m_i \leq M < \infty$, where margin $m_i = y_i \langle \mathbf{w}, \mathbf{x}_i \rangle$. Let $\mathcal{M}, \mathcal{S}, \mathcal{N}$ denote the majority, minority, and noise subsets, respectively. $D = \mathcal{M} \cup \mathcal{S} \cup \mathcal{N}$. We define $\sigma(z) = 1/(1 + \exp^{-z})$.*

\mathcal{D} is a mixture distribution

$$\mathcal{D} = p_{\mathcal{M}} \mathcal{D}_{\mathcal{M}} + p_{\mathcal{S}} \mathcal{D}_{\mathcal{S}} + p_{\mathcal{N}} \mathcal{D}_{\mathcal{N}},$$

with mixture weights $p_{\mathcal{M}} + p_{\mathcal{S}} + p_{\mathcal{N}} = 1$, and $p_{\mathcal{M}} \gg p_{\mathcal{S}}, p_{\mathcal{N}}$. Here, $\mathcal{D}_{\mathcal{M}}$ generates majority samples with $\mathbf{x}_1 = y \boldsymbol{\mu}_1$, $\mathbf{x}_2 \sim \mathcal{N}(0, I_{d_2})$, $\mathbf{x}_3 \sim \mathcal{N}(0, I_{d_3})$ where $\boldsymbol{\mu}_1$ is a fixed vector; $\mathcal{D}_{\mathcal{S}}$ generates

³These results do not consider image transformations (e.g. random crop, rotations), however we have also replicated the experiment with transformations, obtaining a similar trend.

minority samples with $\mathbf{x}_1 = \boldsymbol{\nu}$, $\mathbf{x}_2 = y\boldsymbol{\mu}_2$, $\mathbf{x}_3 \sim \mathcal{N}(0, I_{d_3})$ where $\boldsymbol{\mu}_2$ is a fixed vector and $\boldsymbol{\nu}$ is a random vector anti-aligned with \mathbf{w}_1 ($\langle \mathbf{w}_1, \boldsymbol{\nu} \rangle < 0$); and $\mathcal{D}_{\mathcal{N}}$ generates pure noise samples with $\mathbf{x} \sim \mathcal{N}(0, I_{d_1+d_2+d_3})$. Let $(n_{\mathcal{M}}, n_{\mathcal{S}}, n_{\mathcal{N}})$ denote the counts of majority, minority, and noise samples in S .

Our model easily translates to a logistic regression model if we set $f_{\mathbf{w}}(\mathbf{x}) = \sigma(\langle \mathbf{w}, \mathbf{x} \rangle)$ and change the label to $y \in \{0, 1\}$. The setup in which a part of the input contains the true signal has been commonly used in previous works (Chen et al., 2023; Kou et al., 2023) but we generalize their setup by including and analyzing subclasses in the design. Concretely, one can think of a minority sample as belonging to a long-tail subgroup of the class that requires a different feature to be recognized. We formalize an anti-alignment condition: the minority features are arranged such that any model that heavily prioritizes the majority feature u will perform poorly on the minority. Intuitively, fitting the minority subgroup requires the model to memorize an alternative pattern that is independent of (or even interfering with) the main decision boundary for the majority. We assume the minority subgroup is very small, so that by default a standard empirical risk minimizer might deem it negligible. This resonates with the long-tail phenomena observed in practice – a handful of unusual examples exist that a model could easily ignore without significant impact on overall training loss. However, those examples are crucial for tail generalization: they represent rare yet valid concepts that an ideal model should learn. Our assumptions reflect prior findings that real datasets contain such long-tailed subpopulations which must be memorized to achieve the best possible accuracy Feldman (2020). Formally,

Condition 1. For each minority point $i \in \mathcal{S}$, define

$$B_i := -y_i \langle \mathbf{w}_1, \boldsymbol{\nu}_i \rangle > 0, \quad A := \langle \mathbf{w}_2, \boldsymbol{\mu}_2 \rangle.$$

Let B be a random variable with CDF $F_B(A) = \Pr(B < A)$ such that $B \stackrel{d}{=} B_i$ (i.e., F_B is the law/distribution of the B_i 's when i is drawn uniformly from \mathcal{S}). We assume

$$A < B_{\max}, \quad B_{\max} := \sup\{b \in \mathbb{R} \mid F_B(b) < 1\},$$

This condition assures that the majority feature still dominates globally. Furthermore, we formulate $\boldsymbol{\nu}$ as a random variable to effectively capture multiple atypical subclasses. For example, there can be a wide range of tigers that are purely white or yellowish-white. By modeling $\boldsymbol{\nu}$ as a random variable, it provides variation on the strength of anti-alignment with the majority feature.

Driven by the empirical motivations in Section 4, we define an ordering of the models as how much minority subclass alignment (MSA) they achieved. Formally,

Definition 2 (Minority Subclass Alignment Order). Given two interpolating solutions $\mathbf{w}^{(A)}, \mathbf{w}^{(B)}$ trained on the same S , define

$$A^{(A)} := \langle \mathbf{w}_2^{(A)}, y\boldsymbol{\mu}_2 \rangle, \quad A^{(B)} := \langle \mathbf{w}_2^{(B)}, y\boldsymbol{\mu}_2 \rangle.$$

We write

$$\mathbf{w}^{(A)} \underset{\text{MSA}}{\succcurlyeq} \mathbf{w}^{(B)}$$

and say that $\mathbf{w}^{(A)}$ has higher minority subclass alignment than $\mathbf{w}^{(B)}$ if

$$A^{(A)} \geq A^{(B)} \quad \text{and} \quad A^{(A)}, A^{(B)} < B_{\max}.$$

Now, we formally define attack setup and attacker's advantage for MIA. We focus on the confidence threshold based attack as it is empirically one of the most effective attacks and naturally connected to entropy and modified entropy.

Definition 3 (Confidence-threshold attacker). For $t > 0$ (probabilistic confidence $\tau = \sigma(t)$), define $\mathcal{A}_t(x, y) = \mathbb{1}\{y\langle \mathbf{w}, \mathbf{x} \rangle \geq t\}$ and the attacker's advantage

$$\text{Adv}^M(w, t) := \Pr(\mathcal{A}_t=1 \mid (\mathbf{x}, y) \in D) - \Pr(\mathcal{A}_t=1 \mid (\mathbf{x}, y) \sim \mathcal{D}).$$

where the probability is taken over S .

Note that the attacker's advantage is the difference in the True Positive Rate (TPR) and the False Positive Rate (FPR). Now we state our main results.

Theorem 1 (Higher MSA \implies Better Generalization). *Let $\mathbf{w}^{(A)}, \mathbf{w}^{(B)}$ be two interpolating solutions trained on the same D . Under Definition 1 and regulatory conditions, if $\mathbf{w}^{(A)} \succsim^{\text{MSA}} \mathbf{w}^{(B)}$, then*

$$\Pr(y\langle \mathbf{w}^{(A)}, \mathbf{x} \rangle > 0 \mid (\mathbf{x}, y) \sim \mathcal{D}) \geq \Pr(y\langle \mathbf{w}^{(B)}, \mathbf{x} \rangle > 0 \mid (\mathbf{x}, y) \sim \mathcal{D}),$$

with strict inequality if $F_B([A^{(B)}, A^{(A)}]) > 0$.

Theorem 1 shows that the interpolating model that aligns with the minority subclass feature more generalizes better.

Theorem 2 (Higher MSA \implies Higher Attacker’s Advantage). *Let $\mathbf{w}^{(A)}, \mathbf{w}^{(B)}$ be two interpolating solutions trained on the same D and $\mathbf{w}^{(A)} \succsim^{\text{MSA}} \mathbf{w}^{(B)}$. Choose any threshold $t = \text{logit}(\tau)$ such that*

$$\max\{A^{(A)}, A^{(B)}, m_0^{(A)}, m_0^{(B)}\} < t$$

Then under Definition 1 and regulatory conditions,

$$\text{Adv}^M(\mathbf{w}^{(A)}, t) \geq \text{Adv}^M(\mathbf{w}^{(B)}, t),$$

with strict inequality whenever some minority training indicator at threshold t flips under $\mathbf{w}^{(A)}$ but not under $\mathbf{w}^{(B)}$.

Theorem 2 shows that the model that exhibits higher generalization under our setting can also exhibit higher attacker’s advantage. The condition on the threshold t is easily met in practice as the learned probability threshold $\sigma(t)$ is often high (between 0.9 and 0.98 in our experiments).

6 CONCLUSION AND FUTURE WORK

Our work is an exploration of SAM’s properties pertaining to long-tailed data distributions to unearth surprising tradeoffs between membership privacy risk and generalization. With the insights offered by our experiments and theoretical analysis, we hope to motivate more privacy aware methods in the future.

REFERENCES

Zeyuan Allen-Zhu, Yuanzhi Li, and Yingyu Liang. Learning and generalization in overparameterized neural networks, going beyond two layers. *Advances in neural information processing systems*, 32, 2019.

Christina Baek, Zico Kolter, and Aditi Raghunathan. Why is sam robust to label noise?, 2024. URL <https://arxiv.org/abs/2405.03676>.

Junbum Cha, Sanghyuk Chun, Kyungjae Lee, Han-Cheol Cho, Seunghyun Park, Yunsung Lee, and Sungrae Park. Swad: Domain generalization by seeking flat minima. *Advances in Neural Information Processing Systems*, 34:22405–22418, 2021.

Dingfan Chen, Ning Yu, and Mario Fritz. Relaxloss: Defending membership inference attacks without losing utility, 2022. URL <https://arxiv.org/abs/2207.05801>.

Zixiang Chen, Junkai Zhang, Yiwen Kou, Xiangning Chen, Cho-Jui Hsieh, and Quanquan Gu. Why does sharpness-aware minimization generalize better than sgd?, 2023. URL <https://arxiv.org/abs/2310.07269>.

Jiawei Du, Zhou Daquan, Jiashi Feng, Vincent Tan, and Joey Tianyi Zhou. Sharpness-aware training for free. In Alice H. Oh, Alekh Agarwal, Danielle Belgrave, and Kyunghyun Cho (eds.), *Advances in Neural Information Processing Systems*, 2022.

Xingli Fang and Jung-Eun Kim. Center-based relaxed learning against membership inference attacks, 2024. URL <https://arxiv.org/abs/2404.17674>.

Vitaly Feldman. Does learning require memorization? a short tale about a long tail. In *Proceedings of the 52nd Annual ACM SIGACT Symposium on Theory of Computing*, pp. 954–959, 2020.

Vitaly Feldman and Chiyuan Zhang. What neural networks memorize and why: Discovering the long tail via influence estimation. *Advances in Neural Information Processing Systems*, 33:2881–2891, 2020.

Pierre Foret, Ariel Kleiner, Hossein Mobahi, and Behnam Neyshabur. Sharpness-aware minimization for efficiently improving generalization. *arXiv preprint arXiv:2010.01412*, 2020.

Hongsheng Hu, Zoran Salcic, Lichao Sun, Gillian Dobbie, Philip S Yu, and Xuyun Zhang. Membership inference attacks on machine learning: A survey. *ACM Computing Surveys (CSUR)*, 54(11s):1–37, 2022.

Pavel Izmailov, Dmitrii Podoprikhin, Timur Garipov, Dmitry Vetrov, and Andrew Gordon Wilson. Averaging weights leads to wider optima and better generalization. *arXiv preprint arXiv:1803.05407*, 2018.

Jinyuan Jia, Ahmed Salem, Michael Backes, Yang Zhang, and Neil Zhenqiang Gong. Memguard: Defending against black-box membership inference attacks via adversarial examples. In *Proceedings of the 2019 ACM SIGSAC conference on computer and communications security*, pp. 259–274, 2019.

Minyoung Kim, Da Li, Shell X Hu, and Timothy Hospedales. Fisher SAM: Information geometry and sharpness aware minimisation. In Kamalika Chaudhuri, Stefanie Jegelka, Le Song, Csaba Szepesvari, Gang Niu, and Sivan Sabato (eds.), *Proceedings of the 39th International Conference on Machine Learning*, volume 162 of *Proceedings of Machine Learning Research*, pp. 11148–11161. PMLR, 17–23 Jul 2022.

Yiwen Kou, Zixiang Chen, Yuanzhou Chen, and Quanquan Gu. Benign overfitting for two-layer relu convolutional neural networks, 2023. URL <https://arxiv.org/abs/2303.04145>.

Jungmin Kwon, Jeongseop Kim, Hyunseo Park, and In Kwon Choi. Asam: Adaptive sharpness-aware minimization for scale-invariant learning of deep neural networks. In Marina Meila and Tong Zhang (eds.), *Proceedings of the 38th International Conference on Machine Learning*, volume 139 of *Proceedings of Machine Learning Research*, pp. 5905–5914. PMLR, 18–24 Jul 2021.

Yunhui Long, Vincent Bindschaedler, and Carl A Gunter. Towards measuring membership privacy. *arXiv preprint arXiv:1712.09136*, 2017.

Sasi Kumar Murakonda and Reza Shokri. ML privacy meter: Aiding regulatory compliance by quantifying the privacy risks of machine learning. *arXiv preprint arXiv:2007.09339*, 2020.

Milad Nasr, Reza Shokri, and Amir Houmansadr. Machine learning with membership privacy using adversarial regularization. In *Proceedings of the 2018 ACM SIGSAC conference on computer and communications security*, pp. 634–646, 2018.

Milad Nasr, Reza Shokri, and Amir Houmansadr. Comprehensive privacy analysis of deep learning: Passive and active white-box inference attacks against centralized and federated learning. In *2019 IEEE symposium on security and privacy (SP)*, pp. 739–753. IEEE, 2019.

Matthew D Norton and Johannes O Royset. Diametrical risk minimization: Theory and computations. *Machine Learning*, pp. 1–19, 2021.

Alexandre Sablayrolles, Matthijs Douze, Cordelia Schmid, Yann Ollivier, and Hervé Jégou. White-box vs black-box: Bayes optimal strategies for membership inference. In *International Conference on Machine Learning*, pp. 5558–5567. PMLR, 2019.

Ahmed Salem, Yang Zhang, Mathias Humbert, Pascal Berrang, Mario Fritz, and Michael Backes. ML-leaks: Model and data independent membership inference attacks and defenses on machine learning models. *arXiv preprint arXiv:1806.01246*, 2018.

Reza Shokri, Marco Stronati, Congzheng Song, and Vitaly Shmatikov. Membership inference attacks against machine learning models. In *2017 IEEE symposium on security and privacy (SP)*, pp. 3–18. IEEE, 2017.

Reza Shokri, Martin Strobel, and Yair Zick. On the privacy risks of model explanations. In *Proceedings of the 2021 AAAI/ACM Conference on AI, Ethics, and Society*, pp. 231–241, 2021.

Liwei Song and Prateek Mittal. Systematic evaluation of privacy risks of machine learning models. In *USENIX Security Symposium*, volume 1, pp. 4, 2021.

Xinyu Tang, Saeed Mahloujifar, Liwei Song, Virat Shejwalkar, Milad Nasr, Amir Houmansadr, and Prateek Mittal. Mitigating membership inference attacks by {Self-Distillation} through a novel ensemble architecture. In *31st USENIX Security Symposium (USENIX Security 22)*, pp. 1433–1450, 2022.

Dongxian Wu, Shu-Tao Xia, and Yisen Wang. Adversarial weight perturbation helps robust generalization. *Advances in Neural Information Processing Systems*, 33:2958–2969, 2020.

Samuel Yeom, Irene Giacomelli, Matt Fredrikson, and Somesh Jha. Privacy Risk in Machine Learning: Analyzing the Connection to Overfitting . In *2018 IEEE 31st Computer Security Foundations Symposium (CSF)*, pp. 268–282, Los Alamitos, CA, USA, July 2018. IEEE Computer Society. doi: 10.1109/CSF.2018.00027. URL <https://doi.ieee.org/10.1109/CSF.2018.00027>.

Samuel Yeom, Irene Giacomelli, Alan Menaged, Matt Fredrikson, and Somesh Jha. Overfitting, robustness, and malicious algorithms: A study of potential causes of privacy risk in machine learning. *Journal of Computer Security*, 28(1):35–70, 2020.

Sergey Zagoruyko and Nikos Komodakis. Wide residual networks. *arXiv preprint arXiv:1605.07146*, 2016.

Chiyuan Zhang, Samy Bengio, Moritz Hardt, Benjamin Recht, and Oriol Vinyals. Understanding deep learning (still) requires rethinking generalization. *Communications of the ACM*, 64(3):107–115, 2021.

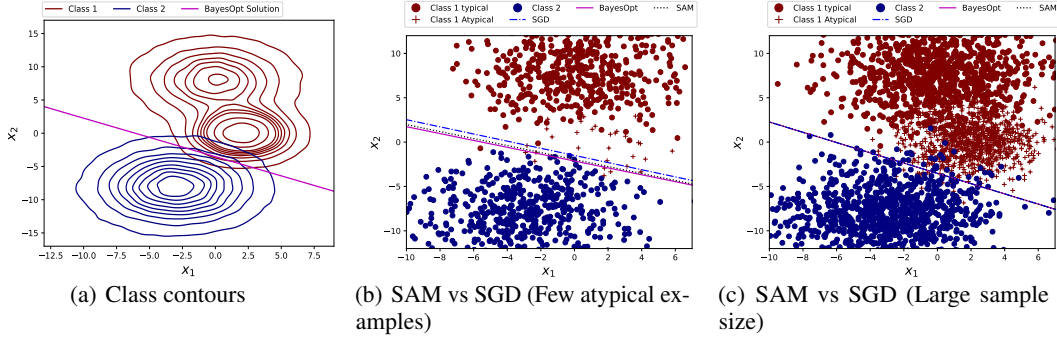


Figure 5: A synthetic construction illustrating the generalization ability of SAM over SGD for atypical examples. Fig (a) shows class density contours of a two-class, 2-dimensional classification problem, along with the Bayes Optimal solution. The red class has two ‘clusters’, one representing typical examples and one representing atypical examples. Fig (b) shows an instance of data sampled from densities shown in (a); the larger cluster of red dots represent typical examples in the red class, and the red ‘+’ points represent a lot fewer atypical examples. SAM generalizes better than SGD in this case. Fig (c) shows that if there are enough samples generated from both typical and atypical clusters, SAM and SGD coincide with the Bayes Optimal classifier.

A LLM USAGE

LLMs were used to assist with grammar correction and sentence-level proofreading throughout the manuscript.

B SYNTHETIC DATASET

In this section, we provide a simple synthetic construction that illustrates how SAM can achieve better generalization performance vs vanilla SGD. The example is illustrated in Figure 5. The data is generated from two-dimensional densities illustrated in Figure 5(a). The densities are supported in two dimensions labelled as x_1 and x_2 . There are two classes - the red class and the blue class. Figure 5(a) also shows the Bayes Optimal classifier. The red class has two ‘clusters’, one representing the typical examples (e.g. yellow tigers), and the other representing the atypical examples (e.g. white tigers). The data is sampled in such a way that we have several samples from the typical cluster, while there are only a few samples from the atypical cluster in the red class. This is shown in Figure 5(b). Figure 5(b) further shows that seeking flatter minima using the SAM optimizer learns a classifier that is closer to the Bayes Optimal classifier than the classifier learnt using vanilla SGD, and thus the former generalizes better. This difference in performance vanishes in Figure 5(c) when we have a large sample size for the atypical examples as well.

This synthetic construction shows that one possible reason that SAM can perform better is if it tends to memorize atypical samples more than vanilla SGD. In other words, the gain in generalization could potentially come from those atypical data subgroups. In the next subsection, we empirically verify this conjecture for the CIFAR-100 dataset.

C PROOFS

Lemma 1 (High-dimensional near-orthogonality). *Let $\mathbf{x}_1, \dots, \mathbf{x}_N \in \mathbb{R}^d$ have i.i.d. $\mathcal{N}(0, 1)$ entries. Then, as $d \rightarrow \infty$,*

$$\|\mathbf{x}_i\|^2 = d(1 + o(1)) \quad \text{and} \quad \frac{\langle \mathbf{x}_i, \mathbf{x}_j \rangle}{\|\mathbf{x}_i\| \|\mathbf{x}_j\|} = o(1)$$

for each fixed $i \neq j$, with probability tending to 1. Moreover, the two conclusions hold uniformly over all $i \neq j$ with probability tending to 1 provided $\log N = o(d)$.

Proof. For norms, $\|\mathbf{x}_i\|^2 \sim \chi^2(d)$. Laurent–Massart’s inequality implies that for all $t > 0$,

$$\Pr(\|\mathbf{x}_i\|^2 - d \geq 2\sqrt{dt} + 2t) \leq e^{-t}, \quad \Pr(d - \|\mathbf{x}_i\|^2 \geq 2\sqrt{dt}) \leq e^{-t}.$$

Taking $t = \varepsilon^2 d$ gives $\|\mathbf{x}_i\|^2 = d(1 \pm O(\varepsilon))$ with probability at least $1 - 2e^{-\varepsilon^2 d}$, hence $\|\mathbf{x}_i\|^2 = d(1 + o(1))$ w.h.p. and $\|\mathbf{x}_i\| = \sqrt{d} + \mathcal{O}_p(1)$.

For inner products, write $\langle \mathbf{x}_i, \mathbf{x}_j \rangle = \sum_{k=1}^d Z_k$ with $Z_k := \mathbf{x}_{i,k} \mathbf{x}_{j,k}$, which are i.i.d., mean 0, and sub-exponential. Bernstein’s inequality yields

$$\Pr(|\langle \mathbf{x}_i, \mathbf{x}_j \rangle| \geq t) \leq 2 \exp\left(-c \min\{t^2/d, t\}\right)$$

for a universal $c > 0$. Taking $t = C\sqrt{d}$ shows $|\langle \mathbf{x}_i, \mathbf{x}_j \rangle| = \mathcal{O}_p(\sqrt{d})$. Combining with $\|\mathbf{x}_i\| \|\mathbf{x}_j\| = d(1 + o_p(1))$,

$$\frac{|\langle \mathbf{x}_i, \mathbf{x}_j \rangle|}{\|\mathbf{x}_i\| \|\mathbf{x}_j\|} = \mathcal{O}_p(d^{-1/2}) = o_p(1).$$

A union bound over the $\binom{N}{2}$ pairs then gives the uniform statement whenever $\log N = o(d)$, since both tails are $\exp(-\Theta(d))$. \square

Noise weights By the representer theorem, write

$$\mathbf{w}_3 = \sum_{j=1}^n \beta_j y_j \mathbf{x}_{3,j}.$$

Then, for any training point i ,

$$y_i \langle \mathbf{w}_3, \mathbf{x}_{3,i} \rangle = \beta_i \|\mathbf{x}_{3,i}\|^2 + \zeta_i, \quad \zeta_i := \sum_{j \neq i} \beta_j y_j y_j \langle \mathbf{x}_{3,j}, \mathbf{x}_{3,i} \rangle.$$

Under Lemma 1, $\|\mathbf{x}_{3,i}\|^2 = (1 \pm o(1)) d_3$ and the cross inner products are $o(\|\mathbf{x}_{3,i}\| \|\mathbf{x}_{3,j}\|) = o(d_3)$

Condition 1. For each minority point $i \in \mathcal{S}$, define

$$B_i := -y_i \langle \mathbf{w}_1, \boldsymbol{\nu}_i \rangle > 0, \quad A := \langle \mathbf{w}_2, \boldsymbol{\mu}_2 \rangle.$$

Let B be a random variable with CDF $F_B(A) = \Pr(B < A)$ such that $B \stackrel{d}{=} B_i$ (i.e., F_B is the law/distribution of the B_i ’s when i is drawn uniformly from \mathcal{S}). We assume

$$A < B_{\max}, \quad B_{\max} \triangleq \sup\{b \in \mathbb{R} \mid F_B(b) < 1\},$$

Remark 1 (Distribution F_B and why $F_B(A)$ appears). For each minority sample i , the anti-alignment magnitude $B_i \triangleq -y_i \langle \mathbf{w}_1, \boldsymbol{\nu}_i \rangle > 0$ summarizes how strongly the majority anchor opposes the minority anchor for that sample. We assume $\{B_i\}_{i \in \mathcal{S}}$ are i.i.d. draws from a common distribution F_B supported on $(0, B_{\max}]$. Unseen minority test point has margin $m' = -B + A + \zeta'$, with $B \sim F_B$, so $\Pr_{\mathcal{S}}(m' > 0) = \Pr(B < A) = F_B(A)$ (up to the $o(1)$ fluctuation ζ' from Lemma 1). Intuitively, $F_B(A)$ is the fraction of minority subclasses whose majority anti-alignment is not too strong relative to the learned shared minority signal A .

Definition 4 (Generalization gap). *The generalization gap for a training point i from distribution $\mathcal{D}_{\mathcal{K}} \in \mathcal{D}_{\mathcal{S}}, \mathcal{D}_{\mathcal{M}}, \mathcal{D}_{\mathcal{N}}$ is defined as*

$$R_i^{\mathcal{K}}(w) := \Pr\{y_i \langle \mathbf{w}, \mathbf{x}_i \rangle > 0\} - \Pr(y' \langle \mathbf{w}, \mathbf{x}' \rangle > 0), \quad (\mathbf{x}', y') \sim \mathcal{D}_{\mathcal{K}}. \quad (7)$$

Assumption 1 (Majority alignment). We consider models whose first block weights align with the majority subclass feature:

$$\mathbf{w}_1 = \alpha \boldsymbol{\mu} \quad (\alpha > 0),$$

This captures the implicit bias of common ERM procedures (e.g., logistic regression trained by gradient descent, or minimum- ℓ_2 -norm interpolation) to align with the dominant signal in the data.

Assumption 2 (Majority dominance). We assume the majority signal dominates the stochastic parts:

$$\frac{\langle \mathbf{w}_1, \boldsymbol{\mu}_1 \rangle^2}{\|\mathbf{w}_2\|^2 + \|\mathbf{w}_3\|^2} \rightarrow \infty.$$

Assumption 3 (Perfect interpolation and finite-margin). A trained model \mathbf{w} has finite margins. That is, there exist $0 < m_0 \leq M < \infty$ such that

$$m_0 \leq y_i \langle \mathbf{w}, \mathbf{x}_i \rangle \leq M \quad \forall i.$$

Assumption 4 (β -stability under higher MSA). Let $w^{(A)}, w^{(B)}$ be interpolating solutions trained on the same S with $A^{(A)} \geq A^{(B)}$. We assume that the per-point coefficient drift of the noise-block representer weights does not offset the threshold shift induced by A ; namely, for every minority point $i \in \mathcal{S}$,

$$\beta_i^{(A)} - \beta_i^{(B)} \geq -\frac{A^{(A)} - A^{(B)}}{\|x_{3,i}\|^2}. \quad (8)$$

Lemma 2 (Generalization gap of majority subclass samples). *Let $i \in \mathcal{M}$. Then with probability $1 - o(1)$,*

$$R_i^{\mathcal{M}}(\mathbf{w}) = o(1)$$

Proof. By Assumption 3, $y_i \langle \mathbf{w}, \mathbf{x}_i \rangle > 0$, hence $\Pr\{y_i \langle \mathbf{w}, \mathbf{x}_i \rangle > 0\} = 1$.

Draw $(x', y') \sim \mathcal{D}_{\mathcal{M}}$, so $x'_1 = y' \mu_1$, $x'_2 \sim \mathcal{N}(0, I_{d_2})$, $x'_3 \sim \mathcal{N}(0, I_{d_3})$, independent of y' . Then

$$y' \langle \mathbf{w}, x' \rangle = \langle \mathbf{w}_1, \mu_1 \rangle + y' \langle \mathbf{w}_2, x'_2 \rangle + y' \langle \mathbf{w}_3, x'_3 \rangle =: \langle \mathbf{w}_1, \mu_1 \rangle + Z,$$

where Z is a mean-zero sub-Gaussian random variable with variance proxy $\text{VarProxy}(Z) = \|\mathbf{w}_2\|^2 + \|\mathbf{w}_3\|^2$, since $y' \langle \mathbf{w}_2, x'_2 \rangle \sim \mathcal{N}(0, \|\mathbf{w}_2\|^2)$ and $y' \langle \mathbf{w}_3, x'_3 \rangle \sim \mathcal{N}(0, \|\mathbf{w}_3\|^2)$ are independent and centered.

For any $a > 0$, a standard sub-Gaussian tail bound yields

$$\Pr\{Z \leq -a\} \leq \exp\left(-\frac{a^2}{2(\|\mathbf{w}_2\|^2 + \|\mathbf{w}_3\|^2)}\right).$$

Taking $a = \langle \mathbf{w}_1, \mu_1 \rangle$,

$$\Pr\{y' \langle \mathbf{w}, \mathbf{x}' \rangle \leq 0\} = \Pr\{Z \leq -\langle \mathbf{w}_1, \mu_1 \rangle\} \leq \exp\left(-\frac{\langle \mathbf{w}_1, \mu_1 \rangle^2}{2(\|\mathbf{w}_2\|^2 + \|\mathbf{w}_3\|^2)}\right).$$

Hence

$$\Pr\{y' \langle \mathbf{w}, \mathbf{x}' \rangle > 0\} \geq 1 - \exp\left(-\frac{\langle \mathbf{w}_1, \mu_1 \rangle^2}{2(\|\mathbf{w}_2\|^2 + \|\mathbf{w}_3\|^2)}\right).$$

By Assumption 2,

$$R_i^{\mathcal{M}}(\mathbf{w}) = 1 - \Pr\{y' \langle \mathbf{w}, \mathbf{x}' \rangle > 0\} \leq \exp\left(-\frac{\langle \mathbf{w}_1, \mu_1 \rangle^2}{2(\|\mathbf{w}_2\|^2 + \|\mathbf{w}_3\|^2)}\right) = o(1)$$

□

Lemma 3 (Generalization gap of minority subclass samples). *Let $i \in \mathcal{S}$.*

$$R_i^{\mathcal{S}}(\mathbf{x}) = 1 - F_B(A) \quad (\text{up to } o(1) \text{ terms}).$$

Proof. By Assumption 3, $y_i \langle \mathbf{w}, \mathbf{x}_i \rangle > 0$, hence $\Pr\{y_i \langle \mathbf{w}, \mathbf{x}_i \rangle > 0\} = 1$.

Draw $(x', y') \sim \mathcal{D}_{\mathcal{S}}$. \mathbf{x}'_3 is independent of $\{\mathbf{x}_{3,j}\}$ and mean-zero; hence $y \langle \mathbf{w}_3, \mathbf{x}'_3 \rangle = \sum_j \beta_j y y_j \langle \mathbf{x}_{3,j}, \mathbf{x}'_3 \rangle$ is a mean-zero fluctuation with variance vanishing relative to $\|\mathbf{x}'_3\|^2$; set this fluctuation to $\zeta' = o_{\mathbb{P}}(1)$ using Lemma 1. Then, $y' \langle \mathbf{w}, \mathbf{x}' \rangle = -B + A + \zeta'$.

$$\Pr\{y' \langle \mathbf{w}, \mathbf{x}' \rangle > 0\} = \Pr\{B < A - \zeta'\} \in (F_B(A - \varepsilon), F_B(A + \varepsilon)).$$

Letting $\varepsilon \downarrow 0$ gives the stated identities up to $o(1)$. □

Lemma 4 (Generalization gap for pure noise samples). *Let $i \in \mathcal{N}$ (pure noise).*

$$R_i^{\mathcal{N}}(\mathbf{w}) = \frac{1}{2}$$

Proof. By Assumption 3, $y_i \langle \mathbf{w}, \mathbf{x}_i \rangle > 0$, hence $\Pr\{y_i \langle \mathbf{w}, \mathbf{x}_i \rangle > 0\} = 1$.

For an unseen noise $(\mathbf{x}', y') \sim \mathcal{D}_{\mathcal{N}}$, each term $y' \langle \mathbf{w}_k, \mathbf{w}'_k \rangle$ ($k = 1, 2, 3$) is a centered continuous symmetric random variable (linear form of a mean-zero isotropic vector, independent of y'). The sum remains centered and symmetric; hence $\Pr\{y' \langle \mathbf{w}, \mathbf{x}' \rangle > 0\} = 1/2$. □

Proof of Theorem 1

Proof. By Lemma 3, minority test accuracy equals $F_B(A)$. This is monotone increasing in A . The majority subclass and noise samples yield the same result for both models by Lemmas 2 and 4. \square

Proof of Theorem 2

Proof. Decompose $\text{Adv}^M = \text{TPR} - \text{FPR}$.

TPR: On training points, **majority subclass samples** exceed any finite fixed t by Assumption 2 and Lemma 2.

For **pure noise samples**, fix any margin threshold $t \geq 0$. For a pure noise training point $i \in \mathcal{N}$,

$$y_i \langle \mathbf{w}, \mathbf{x}_i \rangle = \underbrace{y_i \langle \mathbf{w}_1, \mathbf{x}_{1,i} \rangle + y_i \langle \mathbf{w}_2, \mathbf{x}_{2,i} \rangle}_{G_i} + \underbrace{y_i \langle \mathbf{w}_3, \mathbf{x}_{3,i} \rangle}_{= \beta_i \|\mathbf{x}_{3,i}\|^2 + \zeta_i} = G_i + \beta_i \|\mathbf{x}_{3,i}\|^2 + \zeta_i.$$

Hence the threshold indicator admits the exact identity

$$\mathbb{1}\{y_i \langle \mathbf{w}, \mathbf{x}_i \rangle \geq t\} = \mathbb{1}\left\{\beta_i \geq \frac{t - G_i - \zeta_i}{\|\mathbf{x}_{3,i}\|^2}\right\}.$$

By sub-Gaussianity of $\mathbf{x}_{1,i}, \mathbf{x}_{2,i}$, there exists $r_\eta = \Theta(\|\mathbf{w}_1\| + \|\mathbf{w}_2\|)$ such that

$$\Pr(|G_i| \leq r_\eta) \geq 1 - \eta \quad (\text{for any fixed } \eta \in (0, 1)).$$

By Lemma 1, the remainder $\zeta_i = o_{\mathbb{P}}(1)$; that is, for every $\varepsilon > 0$ there exists a function $\delta_\varepsilon = \delta_\varepsilon(d_3) \downarrow 0$ as $d_3 \rightarrow \infty$ such that

$$\Pr(|\zeta_i| \leq \varepsilon) \geq 1 - \delta_\varepsilon.$$

Intersecting these events, with probability at least $1 - \eta - \delta_\varepsilon$ we have

$$t - r_\eta - \varepsilon \leq t - G_i - \zeta_i \leq t + r_\eta + \varepsilon.$$

Plugging in yields

$$\mathbb{1}\left\{\beta_i \geq \frac{t + r_\eta + \varepsilon}{\|\mathbf{x}_{3,i}\|^2}\right\} \leq \mathbb{1}\{y_i \langle \mathbf{w}, \mathbf{x}_i \rangle \geq t\} \leq \mathbb{1}\left\{\beta_i \geq \frac{t - r_\eta - \varepsilon}{\|\mathbf{x}_{3,i}\|^2}\right\},$$

holding with probability $1 - \eta - \delta_\varepsilon$. Letting $\varepsilon \downarrow 0$ and using $\|\mathbf{x}_{3,i}\|^2 = (1 \pm o(1))d_3$, define the data-dependent thresholds

$$\tau_i^{(+)}(t) := \frac{t + r_\eta}{\|\mathbf{x}_{3,i}\|^2}, \quad \tau_i^{(-)}(t) := \frac{t - r_\eta}{\|\mathbf{x}_{3,i}\|^2},$$

so that, with probability $1 - \eta - o(1)$,

$$\mathbb{1}\{\beta_i \geq \tau_i^{(+)}(t)\} \leq \mathbb{1}\{y_i \langle \mathbf{w}, \mathbf{x}_i \rangle \geq t\} \leq \mathbb{1}\{\beta_i \geq \tau_i^{(-)}(t)\}.$$

Therefore, the contribution of pure noise samples on TPR is not dependent on A . Under our setup, higher A likely implies higher $\|\mathbf{w}_2\|$, increasing the required minimum for β_i . Higher β_i can push the sample more above the threshold increasing TPR, more in line with our theorem. This effect, however, is much smaller than the effect from A for minority subclass samples as it affects through $r_\eta = \Theta(\|\mathbf{w}_1\| + \|\mathbf{w}_2\|)$. Also by Assumption 4, the difference in A dominates.

For **minority subclass samples**,

$$m_i = y_i \langle \mathbf{w}, \mathbf{x}_i \rangle = -B_i + S + \beta_i \|\mathbf{x}_{3,i}\|^2 + \zeta_i.$$

Setting $m_i > t$ and rearranging, the total contribution of minority examples is

$$\frac{1}{n_S} \sum_{i \in S} \mathbb{1} \left\{ \beta_i \geq \frac{t - (-B_i + A)}{\|x_{3,i}\|^2} \right\},$$

which is pointwise nondecreasing in A . Hence $\text{TPR}^{(A)} \geq \text{TPR}^{(B)}$, with strict gain when at least one minority indicator flips. That is, if for $i \in S$,

$$\exists i \ m_i^{(B)} < t < m_i^{(A)}$$

FPR: For nonmembers, the mixture \mathcal{D} splits into majority, minority, and noise. At a fixed t , the majority and noise tails do not depend on A . The minority nonmember term equals $F_B(A - t) + o(1)$ (Lemma 3). If $t > \max\{A^{(A)}, A^{(B)}\}$ and $B > 0$ a.s., then $F_B(A^{(A)} - t) = F_B(A^{(B)} - t) = 0$, so the minority part vanishes for both models. Therefore $\text{FPR}^{(A)} = \text{FPR}^{(B)} + o(1)$.

Combining, $\text{Adv}^M(\mathbf{w}^{(A)}, t) \geq \text{Adv}^M(\mathbf{w}^{(B)}, t)$, with strict inequality whenever some minority training indicator flips for $\mathbf{w}^{(A)}$ but not for $\mathbf{w}^{(B)}$. \square

D ADDITIONAL RELATED WORKS

D.1 CONNECTION OF FLATTER MINIMA WITH GENERALIZATION GAP

There have been numerous studies (Foret et al., 2020; Izmailov et al., 2018; Cha et al., 2021; Norton & Royset, 2021; Wu et al., 2020) which account for the worst-case empirical risks within neighborhoods in parameter space. Diametrical Risk Minimization (DRM) was first proposed by (Norton & Royset, 2021) and they asserted that the practical and theoretical performance of Empirical Risk Minimization (ERM) tends to suffer when dealing with loss functions that exhibit poor behavior characterized by large Lipschitz moduli and spurious sharp minimizers. They tackled this concern by employing DRM, which offers generalization bounds that are unaffected by Lipschitz moduli, applicable to both convex and non-convex problems. Another algorithm that improves generalization is Sharpness Aware Minimization (SAM) (Foret et al., 2020) which performs gradient descent while regularizing for the highest loss in the neighborhood of radius ρ of the parameter space. (Izmailov et al., 2018) proposed Stochastic Weight Averaging (SWA) that performs averaging of weights with a cyclical or constant learning rate which leads to better generalization than conventional training. They also prove that the optima chosen by the single model is in fact a flatter minima than the SGD solution. Further, (Cha et al., 2021) argues that simply performing the Empirical Risk Minimization (ERM) is not enough to achieve a good generalization, in particular, domain generalization. Hence, they introduce SWAD which seeks for flatter optima and hence, will generalize well across domain shifts.

D.2 DIFFERENT MEMBERSHIP INFERENCE ATTACKS

There are many variants of Direct Single-query attacks (DSQ) based on the approach of the attack and below we describe the ones used in our experiments:

NN-based attack (Shokri et al., 2017; Tang et al., 2022; Nasr et al., 2018) This is the first MIA proposed by Shokri et al. (2017) where they use a binary classifier to distinguish between the training members and the non-members using the victim model's behavior on these data points. The adversary can utilize the prediction vectors from the target model and incorporate them along with the one-hot encoded ground truth labels as inputs. Then, they can construct a neural network (I_{NN}) called attack model.

Confidence-based attack (Yeom et al., 2020; Salem et al., 2018; Song & Mittal, 2021) If the highest prediction confidence of an input record exceeds a predetermined threshold, the adversary considers it a member; otherwise, it is inferred as a non-member. This approach is based on the understanding that the target model is trained to minimize prediction loss using its training data, implying that the maximum confidence score of a prediction vector for a training member should be near 1. The attack I_{conf} is defined as follows:

$$I_{conf} \hat{p}(y|x) = \mathbb{1}(\max \hat{p}(y|x) \geq \tau) \quad (9)$$

Here, $\mathbb{1}(\cdot)$ is an indicator function which returns 1 if the predicate inside it holds True else the function evaluates to 0.

Entropy-based attack (Nasr et al., 2019; Song & Mittal, 2021; Tang et al., 2022) When the prediction entropy of an input record falls below a predetermined threshold, the adversary considers it a member. Conversely, if the prediction entropy exceeds the threshold, the adversary infers that the record is a non-member. This inference is based on the observation that there are notable disparities in the prediction entropy distributions between training and test data. Typically, the target model exhibits higher prediction entropy on its test data compared to its training data. The entropy of a prediction vector $p(\hat{y}|x)$ is defined as follows:

$$H(p(\hat{y}|x)) = - \sum_i (p_i \log(p_i)) \quad (10)$$

where p_i is the confidence score in $p(\hat{y}|x)$. Then, the attack I_{entr} is given as:

$$I_{entr}(\hat{p}(y|x), y) = \mathbb{1}(H(p(\hat{y}|x)) \leq \tau) \quad (11)$$

Modified entropy-based attack (Song & Mittal, 2021) Song et al.[15] introduced an enhanced prediction entropy metric that integrates both the entropy metric and the ground truth labels. The modified entropy metric tends to yield lower values for training samples compared to testing samples. To infer membership, either a class-dependent threshold τ_y or a class-independent threshold τ_{attack} is applied.

$$I_{Mentr}(\hat{p}(y|x), y) = \mathbb{1}(Mentr(p(\hat{y}|x)) \leq \tau_y) \quad (12)$$

where $Mentr(p(\hat{y}|x))$ for (x,y) data sample is given by combination of entropy information and ground truth label as:

$$Mentr(p(\hat{y}|x)) = -((1 - p(\hat{y}|x)_y) \log(p(\hat{y}|x)_y) - \sum_{i \neq y} (p(\hat{y}|x)_i \log(1 - p(\hat{y}|x)_i))) \quad (13)$$

E DATASETS

Here we introduce the four benchmark datasets used in the experiments and they have been widely used in prior works on MI attacks:

CIFAR-10⁴ This is a benchmark dataset for image classification task. The dataset consists of 60,000 color images of 32x32 size. There are 6,000 images from 10 classes where 5,000 images per class belong to the training dataset and 1,000 images per class belong to the test dataset.

CIFAR-100⁵ The dataset is designed to be more challenging than CIFAR-10 as it contains a greater number of classes and more fine-grained distinctions between objects. There are a total of 60,000 images from 100 classes. Each subclass consists of 600 images, and within each subclass, there are 500 training images and 100 testing images. This distribution ensures a balanced representation of each class in both the training and testing sets.

Purchase-100⁶ This a 100 class classification task with 197,324 data samples and consists of 600 binary feature; each dimension corresponds to a product and its value states if corresponding customer purchased the product; the corresponding label represents the shopping habit of the customer. We use the pre-processed and simplified version provided by Shokri et al. (2017) and used by Tang et al. (2022).

Texas-100⁷ This dataset is based on the Hospital Discharge Data public files with information about inpatients stays in several health facilities released by the Texas Department of State Health Services from 2006 to 2009. We used a prepossessed and simplified version of this dataset provided by (Shokri et al., 2017) and used by (Tang et al., 2022) which is composed of 67,330 data samples with 6,170 binary features. Each feature represents a patient's medical attribute like the external causes of injury, the diagnosis and other generic information. The classification task is to classify patients into 100 output classes which represent the main procedure that was performed on the patient.

⁴<https://www.cs.toronto.edu/~kriz/cifar.html>

⁵<https://www.cs.toronto.edu/~kriz/cifar.html>

⁶<https://www.kaggle.com/c/acquire-valued-shoppers-challenge>

⁷<https://www.dshs.texas.gov/THCIC/Hospitals/Download.shtm>

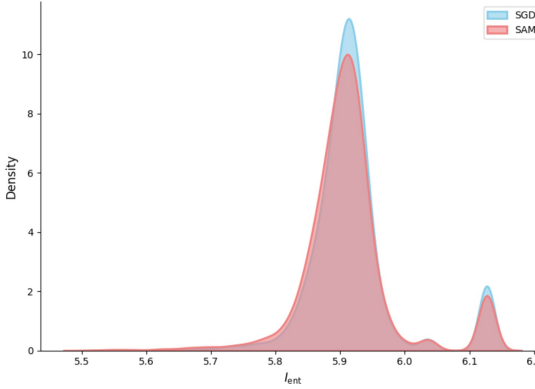


Figure 6: \mathcal{I}_{ent} distribution excluding bucket 5 for SGD and SAM

EyePacs⁸ The pre-processed version of this dataset is obtained from Kaggle and it was originally used for a Diabetic Retinopathy Detection challenge. The dataset consists of 88,702 colour fundus images, including 35,126 samples for training and 53,576 samples for testing. The images were captured under various conditions by various devices at multiple primary care sites throughout California and elsewhere. For each subject, two images of the left and right eyes were collected, with the same resolution. A clinician was asked to rate each image for the presence of DR with a scale of 0–4 according to the Early Treatment Diabetic Retinopathy Study (ETDRS) scale. Note that for this dataset only training set (35k images) is used since the labels for testing set is not publicly available. The images in the dataset vary in their image resolution and we resized all the images to 128x128 pixels for our experiments.

F EXPERIMENTAL SETUP

F.1 MODELS

For CIFAR-100 and CIFAR-10, we use WideResNet (WRN) (Zagoruyko & Komodakis, 2016) with 16 layer depth and 8 as width factor. For Purchase-100 and Texas-100, we follow the setting in Tang et al. (2022) and use a 4-layer fully connected neural network with layer sizes [1024, 512, 256, 100]. For EyePacs, we use ResNet-18.

F.2 \mathcal{I}_{ent} EXPERIMENT

Here we discuss how test data points were grouped into 5 buckets according to different \mathcal{I}_{ent} levels. Bucket 5 contains highest \mathcal{I}_{ent} level, and is composed of test points where all 500 training points have 0 influence score. This means that the prediction output for that test point does not change had the model been trained without any one particular training data point. Because influence scores for all training points are equal, these test points have highest \mathcal{I}_{ent} ⁹. Figure 6 displays distribution of \mathcal{I}_{ent} for remaining test data points. We group those above 6.1 into bucket 4. For the rest of the points, we calculate the mean and standard deviation and use them for grouping. We group points below -0.4σ from the mean into bucket 1, points between -0.4σ and 0.4σ into bucket 2, and points above 0.4σ into bucket 3. Final number of test points in each buckets are [Bucket 1: 1924, Bucket 2: 2996, Bucket 3: 2392, Bucket 4: 535, Bucket 5: 2153]. For SAM’s buckets, final number of test points are [Bucket 1: 1913, Bucket 2: 3181, Bucket 3: 2548, Bucket 4: 502, Bucket 5: 1856]. Number of overlapping indices were [Bucket 1: 1116, Bucket 2: 1625, Bucket 3: 1199, Bucket 4: 133, Bucket 5: 1678].

⁸<https://www.kaggle.com/datasets/mariaherrerot/eyepacspreprocess>

⁹When actually calculating \mathcal{I}_{ent} with Equation (6), this evaluates to 0 due to probability normalization, but represents highest value.

F.3 ATTACK SETUP & SIZE OF DATA SPLITS

We adopt the attack setting from (Tang et al., 2022; Nasr et al., 2018) to determine the partition between training data and test data and to determine the subset of the training and test data that constitutes attacker’s prior knowledge for CIFAR-100, Purchase-100 and Texas-100 datasets. We use similar strategy to determine the data split for CIFAR-10. Specifically, the attacker’s knowledge corresponds to half of the training and test data, and the MIA success is evaluated over the remaining half.

F.4 HYPERPARAMETER TUNING AND EMPIRICAL VALIDATION OF FLATNESS FOR SHARP

For the Sharp objective, we fine-tuned β and ρ that resulted in a model that exhibited sufficient difference in test accuracy and sharpness of the minima compared to SAM and SGD. The final hyperparameters of the model reported were $\rho = 0.01, \beta = 0.6818$ for CIFAR-100 and CIFAR-10, $\rho = 0.01, \beta = 0.83$ for Purchase-100, $\rho = 0.001, \beta = 0.513$ for Texas-100, and $\rho = 0.001, \beta = 0.18$ for EyePacs.

To verify that Sharp actually finds a sharper minima, we computed the trace of the hessian matrix using Hutchinson’s method for SGD, SAM, and Sharp models on CIFAR-100. The results are in Table 2. Higher trace indicates a sharper minima and vice versa. The trace is the largest for Sharp and smallest for SAM.

Method	Trace of the Hessian
Sharp	1556.54
SGD	307.87
SAM	84.18

Table 2: Comparison of Hessian trace values across methods.

F.4.1 BALL OF RADIUS ρ

For SAM loss, sharp minima loss, and our proposed loss, we approximate the maximum loss in the ball of radius ρ around the minima. Norton & Royston (2021) have found that the type of norm that is used for defining the ball has large impact along with actual ρ value. For all our experiments, we use L2 norm for our ball of radius ρ .

F.4.2 HYPERPARAMETER TUNING FOR CIFAR-10 & CIFAR-100

We trained each model for 200 epochs and chose the model with highest validation accuracy on a held-out validation set. We used initial learning rate of 0.1 with learning rate decay of 0.2 at 60th, 120th, and 160th epoch with batch size of 128. We trained the models with weight decay 0.0005 and Nesterov momentum of 0.9. For SWA on CIFAR-100, we trained first 150 epoch with vanilla SGD and used weight averaging for the rest of the epochs.

F.4.3 HYPERPARAMETER TUNING FOR TEXAS-100 & PURCHASE-100

We chose the best model as discussed before for CIFAR-10/100. We trained models with a learning rate of 0.1 with weight decay 0.0005 and Nesterov momentum of 0.9. We trained the models on Purchase-100 for a total of 100 epochs and on Texas-100 for a total of 75 epochs. During training, we employed a batch size of 512 for the Purchase-100 dataset and a batch size of 128 for the Texas-100 dataset.

F.4.4 HYPERPARAMETER TUNING FOR EYEPACS

We trained ResNet-18 with SGD, SAM and our proposed loss using EyePacs dataset for 100 epochs. Since, the dataset is highly imbalanced with about 25k data points out of 35k training data points belonging to one of the five classes, we used the balanced batch sampling strategy and a lower learning rate of 0.01 with learning rate decay of 0.2 at 60th epoch. As before, we also used weight

Table 3: Privacy vs Generalization tradeoff for SAM and SGD using InceptionV4 and Resnet18

Dataset	Model	Optimizer	Test Acc	Best Attack Acc
CIFAR-100	Resnet18	SGD	78.42%	74.31%
		SAM	78.74%	77.45%
	InceptionV4	SGD	77.44%	77.22%
		SAM	79.60%	80.82%
CIFAR-10	Resnet18	SGD	95.18%	57.90%
		SAM	96.16%	60.05%
	InceptionV4	SGD	94.26%	61.60%
		SAM	95.76%	64.41%

decay 0.0005 and Nesterov momentum of 0.9. For our experiments, we utilized a batch size of 100, consisting of 12 samples from each of the 5 classes.

G ABLATION STUDY: COMPARISON OF DIFFERENT ARCHITECTURES

To validate consistency across different model architectures, we report results in Table 3 using InceptionV4¹⁰ and resnet18¹¹ for CIFAR-100 and CIFAR-10. We kept our ρ the same across all model architectures with value 0.1. The results are consistent with our findings that SAM tends to have higher test accuracy while having higher membership attack accuracy at the same time. Overall best attack accuracy is higher for SAM for all the cases although we find mixed findings for multi-query attack accuracy specifically.

¹⁰<https://github.com/weiaicunzai/pytorch-cifar100/blob/master/models/>

¹¹<https://github.com/inspire-group/MIAdefenseSELENA/tree/main>